Occlusion-Aware Riemannian GDOP Coverage Optimization for Lunar Base Positioning Using Mobile Pseudolites

1st Junwu Wang
School of Electrical Engineering and Automation
Anhui University
Hefei, China
z125221066@stu.ahu.edu.cn

2nd Yishi Wang
Shanghai Institute of Aerospace System Engineering
Shanghai 201109, China
nucwangyishi@163.com

3rd Yuxuan Hu
School of Electrical Engineering and Automation
Anhui University
Hefei, China
hyxgcr@163.com

4th Liang Zhang*
School of Electrical Engineering and Automation
Anhui University
Hefei, China
liangzhang@ahu.edu.cn
*Corresponding author

***Abstract*—This paper formulates occlusion-aware regional positioning coverage for lunar base construction using rover-mounted pseudolites. Surface-constrained geometric dilution of precision (GDOP) evaluates positioning geometry for a user state with two surface position coordinates and a receiver clock bias. A bounded service utility combines GDOP with low-service branches for insufficient observations and rank-deficient geometry, and is integrated against a normalized geodesic Gaussian demand field. Hard line-of-sight tests account for lunar body obstruction and two artificial convex obstacles. Established derivative-free particle swarm optimization (PSO) searches feasible static deployments on a lunar south polar spherical cap, subject to domain, obstacle, and inter-rover separation constraints. Twenty independent trials with 6000 objective evaluations each yielded a mean final objective of 0.780976 and a sample standard deviation of 0.005668.**

***Index Terms*—geometric dilution of precision, lunar surface positioning, mobile pseudolites, particle swarm optimization, Riemannian geometry**

I. Introduction

Lunar base construction requires positioning, navigation, and timing services under limited Earth-based support. NASA's LunaNet framework and ESA's Moonlight initiative address cislunar communication and navigation infrastructure [1], [2]. Surface positioning architectures include lunar constellations and joint Doppler and ranging systems [3], [4].

Surface pseudolites complement orbital infrastructure for regional lunar positioning; Fig. 1 illustrates a rover-mounted implementation. Wallace *et al.* analyzed placement, antenna elevation, terrain visibility, and transmitter geometry around Shackleton crater [5]. Toldbo *et al.* considered terrain-dependent lunar beacon placement and evaluated landing geometry through dilution of precision (DOP) [6]. Tang *et al.* used multiobjective PSO for terrestrial pseudolite deployment with digital elevation model (DEM) data and mean horizontal dilution of precision (HDOP) [7].

Coverage control optimizes spatially distributed services using mobile agents [8], and sensor placement can use Fisher-information criteria [9]. Zhang *et al.* used position dilution of precision (PDOP) to guide distributed robot deployment over a planar hotspot [10]. For lunar deployment, the service model must also account for surface constraints, curvature-limited line of sight, terrain feasibility, and receiver clock bias.

Riemannian coverage models incorporate intrinsic geometry, boundaries, and obstacles. Bhattacharya *et al.* generalized coverage to Riemannian manifolds [11], and subsequent work considered deployment on curved, nonconvex surfaces [12]. These objectives emphasize spatial or travel-related service metrics. Regional positioning coverage requires a model that couples hard visibility, clock-bias-aware pseudorange geometry, and nonuniform demand.

This paper integrates hard visibility and surface-constrained geometric dilution of precision (GDOP) in a demand-weighted coverage objective. The user state includes two tangential position coordinates and a receiver clock bias, with low-service branches for insufficient observations and degenerate geometry. An established derivative-free particle swarm optimization (PSO) solver searches feasible static rover configurations. Twenty independent trials evaluate deployment outcomes under stochastic initialization and a fixed search budget.

II. Lunar Surface Positioning Model

A. Lunar Surface Geometry and Pseudorange Model

Rover-mounted pseudolites have known positions and are synchronized to a common network time reference. The

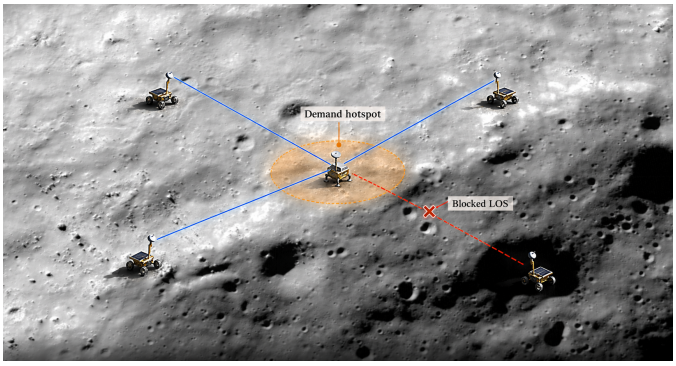

Fig. 1. Conceptual rover-mounted pseudolite deployment. Blue links indicate visible observations; the red link indicates occlusion. Selected rovers illustrate deployment capability; arrows are schematic and do not depict simulated trajectories. Background adapted from NASA/GSFC/SVS LROC imagery (data: Arizona State University); overlays are not to scale.

receiver's surface position and clock bias relative to this reference are unknown.

The lunar surface is modeled as the two-dimensional sphere $\mathcal{M} = S_R^2$ of radius R, with service domain $\Omega \subset \mathcal{M}$. The N pseudolite surface positions are $P = \{\mathbf{p}_1, \ldots, \mathbf{p}_N\}$, with $\mathbf{p}_i \in \mathcal{M}$. Rover placement uses surface geometry, while radionavigation signals propagate along straight three-dimensional segments. For transmitting antenna height h_b, the phase center of pseudolite i is

$$\mathbf{a}_i = \left(1 + \frac{h_b}{R}\right) \mathbf{p}_i. \tag{1}$$

For a user at $\mathbf{q} \in \Omega$ with receiving antenna height h_u, the receiver phase center is

$$\mathbf{x}(\mathbf{q}) = \left(1 + \frac{h_u}{R}\right) \mathbf{q}. \tag{2}$$

Following the one-way pseudorange model in [5], measurement z_i is

$$z_i = r_i + b + \varepsilon_i, \qquad r_i = \|\mathbf{x}(\mathbf{q}) - \mathbf{a}_i\|, \tag{3}$$

where r_i is the range between phase centers, b is the receiver clock bias in distance units, and ε_i is the pseudorange error. For the equal-weight GDOP interpretation, errors are taken to have zero mean, common variance σ_r^2, and no cross-correlation. The simulations evaluate geometry without generating noisy pseudoranges or receiver-position estimates.

Hard line-of-sight (LOS) visibility is denoted by $\chi_i(\mathbf{q}, P) \in \{0, 1\}$. An observation is available only when the complete segment between $\mathbf{a}_i$ and $\mathbf{x}(\mathbf{q})$ is unobstructed by the lunar body and terrain obstacles. The number of visible pseudolites is

$$n(\mathbf{q}, P) = \sum_{i=1}^{N} \chi_i(\mathbf{q}, P). \tag{4}$$

B. Surface-Constrained State and Dilution of Precision

A user known to lie on the lunar surface has two independent position coordinates. Define an orthonormal tangent basis

$$\begin{aligned} B(\mathbf{q}) &= [\mathbf{b}_1(\mathbf{q})\ \mathbf{b}_2(\mathbf{q})], \\ B^{\mathsf{T}}(\mathbf{q})B(\mathbf{q}) &= I_2, \qquad B^{\mathsf{T}}(\mathbf{q})\mathbf{q} = 0. \end{aligned} \tag{5}$$

Its columns span $T_{\mathbf{q}}\mathcal{M}$, the tangent space of the surface [13]. A small surface displacement is described by local coordinates ξ_1 and ξ_2, yielding the state

$$\boldsymbol{\theta} = [\xi_1\ \xi_2\ b]^{\mathsf{T}}. \tag{6}$$

The unit LOS vector from the transmitter to the receiver is

$$\mathbf{e}_i = \frac{\mathbf{x}(\mathbf{q}) - \mathbf{a}_i}{\|\mathbf{x}(\mathbf{q}) - \mathbf{a}_i\|}. \tag{7}$$

Linearizing the pseudorange with respect to the local state gives

$$\delta z_i = \mathbf{g}_i^{\mathsf{T}} \delta\boldsymbol{\theta} + \varepsilon_i, \tag{8}$$

with geometry vector

$$\mathbf{g}_i = \begin{bmatrix} \left(1 + \dfrac{h_u}{R}\right) B^{\mathsf{T}}(\mathbf{q})\mathbf{e}_i \\ 1 \end{bmatrix}. \tag{9}$$

The first two components describe tangential position sensitivity, and the final component describes clock-bias sensitivity. Antenna height enters both the range and the position Jacobian. Stack the visible rows as $G_h = [\mathbf{g}_{i_1}\ \cdots\ \mathbf{g}_{i_n}]^{\mathsf{T}}$, where $\chi_{i_j}(\mathbf{q}, P) = 1$. The geometric information matrix is

$$A_h = G_h^{\mathsf{T}} G_h. \tag{10}$$

Finite GDOP requires $\operatorname{rank}(A_h) = 3$. With $Q = A_h^{-1}$, the stated error model gives the local linear least-squares covariance $\sigma_r^2 Q$. Surface-constrained GDOP is defined as

$$D(\mathbf{q}; P) = \sqrt{\operatorname{tr}(Q)}. \tag{11}$$

This dimensionless GDOP characterizes geometric error amplification in the two surface coordinates and receiver clock bias, and is invariant to rotations of the orthonormal tangent basis.

Numerical rank is computed by counting singular values s_k of G_h that satisfy $s_k > \tau_r s_1$, with $\tau_r = \epsilon_{\text{mach}} \max(N, 3) = 2.220446049250313 \times 10^{-15}$ for $N = 10$ in double precision. At least three visible observations are required for full rank. Configurations with fewer observations or deficient rank use the service branches in Section III without matrix inversion.

III. Occlusion-Aware Positioning Coverage Optimization

A. Regional Service Utility and Coverage Objective

A normalized geodesic Gaussian represents positioning demand over Ω, with center $\mathbf{q}_h$ and width σ_h:

$$\rho(\mathbf{q}) = Z_\rho^{-1} \exp\left[-\frac{d_g^2(\mathbf{q},\mathbf{q}_h)}{2\sigma_h^2}\right],$$
$$Z_\rho = \int_\Omega \exp\left[-\frac{d_g^2(\mathbf{s},\mathbf{q}_h)}{2\sigma_h^2}\right] \mathrm{d}\mu_g(\mathbf{s}), \qquad (12)$$
$$\int_\Omega \rho(\mathbf{q})\,\mathrm{d}\mu_g(\mathbf{q}) = 1,$$

where d_g is spherical geodesic distance and $\mathrm{d}\mu_g$ is the surface area measure. To include insufficient observations and degenerate geometry, define

$$\bar{f}(\mathbf{q},P) = \begin{cases} \nu_0, & n = 0, \\ \nu_1, & n = 1, \\ \nu_2, & n = 2, \\ \nu_3, & n \geq 3,\ \mathrm{rank}(A_h) < 3, \\ f(D(\mathbf{q};P)), & \mathrm{rank}(A_h) = 3, \end{cases} \qquad (13)$$

where $n = n(\mathbf{q},P)$ and $\nu_0 < \nu_1 < \nu_2 < \nu_3$. For full-rank geometry, the continuous, monotonically decreasing map f assigns larger utility to smaller GDOP. The regional objective retains the complete domain, including low-demand blind regions and users with insufficient observations:

$$H(P) = \int_\Omega \rho(\mathbf{q})\bar{f}(\mathbf{q},P)\,\mathrm{d}\mu_g(\mathbf{q}), \qquad \max_P H(P). \qquad (14)$$

Deployment is constrained by the lunar domain, nontraversable obstacle footprints, and minimum inter-rover geodesic separation. The utility and its regional average H quantify geometry-based positioning service, including receiver clock-bias sensitivity.

B. Constrained Rover Deployment via Particle Swarm Optimization

PSO [14] performs a centralized offline search for static rover configurations using objective values. Each particle jointly represents all N rover positions; particle velocities and iterations describe numerical search updates. Let $\mathbf{q}_0$ be the south pole point, $\|\mathbf{q}_0\| = R$, with tangent basis $E_0 = [\mathbf{e}_1^0\ \mathbf{e}_2^0]$, $E_0^\mathsf{T} E_0 = I_2$, and $E_0^\mathsf{T}\mathbf{q}_0 = 0$. Define

$$\mathbf{u}_i = [x_i\ y_i]^\mathsf{T}, \qquad \mathbf{z} = [\mathbf{u}_1^\mathsf{T},\ldots,\mathbf{u}_N^\mathsf{T}]^\mathsf{T} \in \mathbb{R}^{2N}. \qquad (15)$$

The coordinate vector $\mathbf{u}_i$ specifies rover i through the Riemannian exponential map [13]:

$$\mathbf{p}_i = \mathrm{Exp}_{\mathbf{q}_0}(E_0\mathbf{u}_i). \qquad (16)$$

For $\eta_i = \|\mathbf{u}_i\| > 0$, the exact spherical decoding is

$$\mathbf{p}_i = \cos\Big(\frac{\eta_i}{R}\Big)\,\mathbf{q}_0 + R\frac{\sin(\eta_i/R)}{\eta_i}E_0\mathbf{u}_i. \qquad (17)$$

At $\eta_i = 0$, set $\mathbf{p}_i = \mathbf{q}_0$.

A candidate is feasible when every rover lies in Ω, remains outside obstacle footprints, and satisfies the minimum geodesic separation from the other rovers. Infeasible proposals are rejected, retaining the previous feasible particle position.

For each feasible configuration, (1) and (2) reconstruct the antenna phase centers. At every integration point, complete segments are tested against the lunar body and both three-dimensional convex obstacles. The resulting observation set and geometry rank determine the service branch in (13). The hard LOS test has no range cutoff or smoothing.

For each closed occluding ball with center $\mathbf{C}_j$ and radius r_j, let d_j be the minimum distance from $\mathbf{C}_j$ to the closed antenna segment. Visibility requires, for every ball,

$$\kappa_j = \frac{d_j^2 - r_j^2}{2r_j} > \tau_j, \qquad (18)$$
$$\tau_j = 8\epsilon_{\mathrm{mach}}\big[\max(\|\mathbf{a}_i\|,\|\mathbf{x}\|) + \|\mathbf{C}_j\| + r_j\big].$$

The lunar ball has $\mathbf{C}_0 = \mathbf{0}$ and $r_0 = R$. Tangency, contacts within the floating-point guard, and endpoint intersections are blocked.

Positive surface area quadrature weights approximate (14), giving numerical fitness

$$\widehat{H}(P) = \sum_{\ell=1}^{L} w_\ell \rho(\mathbf{q}_\ell)\bar{f}(\mathbf{q}_\ell,P), \qquad (19)$$

where L is the number of integration nodes and w_ℓ is their area weight. All particles use the same integration rule and demand normalization. Low service and rank deficiency follow (13); nonfinite values or unresolved integration errors are recorded as technical failures.

Let $\mathbf{z}_m^{(t)}$ denote particle m's search vector, $\mathbf{v}_m^{(t)}$ its search velocity, $\mathbf{z}_m^{\mathrm{pbest}}$ its personal best, and $\mathbf{z}^{\mathrm{gbest}}$ the swarm best. The inertia-weight PSO formulation [15] uses inertia ω, attraction coefficients c_1, c_2, and independent uniform random vectors $\mathbf{r}_{1,m}, \mathbf{r}_{2,m}$:

$$\mathbf{v}_m^{(t+1)} = \omega\mathbf{v}_m^{(t)} + c_1\mathbf{r}_{1,m} \odot (\mathbf{z}_m^{\mathrm{pbest}} - \mathbf{z}_m^{(t)}) + c_2\mathbf{r}_{2,m} \odot (\mathbf{z}^{\mathrm{gbest}} - \mathbf{z}_m^{(t)}), \qquad (20)$$
$$\mathbf{z}_m^{\mathrm{trial}} = \mathbf{z}_m^{(t)} + \mathbf{v}_m^{(t+1)},$$

where $\odot$ denotes componentwise multiplication. Feasible proposals are evaluated using (19), and personal and global bests are updated for larger fitness values. The stored best fitness is nondecreasing on the fixed search grid.

Algorithm 1. Static configuration search

1) Fix the scene, integration rule, PSO settings, evaluation budget, and random seed.
2) Initialize a feasible swarm; evaluate all particles and initialize their personal and swarm bests.
3) Propose a particle update using (20).
4) Decode its surface positions and check feasibility. Reject unsafe proposals; evaluate feasible ones using hard LOS and (19).
5) Update the stored bests and record the best configuration and its spherical service value.
6) Repeat within the evaluation budget and generation ceiling; return the best feasible configuration found.

Initial fitness evaluations count toward the budget; rejected or cached proposals do not count as new evaluations. A partial generation is recorded when the budget is reached. The generation ceiling bounds execution under repeated infeasibility.

IV. Static Simulation and Statistical Evaluation

A. Simulation Setup

The experiment uses an ideal lunar south polar cap of 50 km geodesic radius, ten rover-mounted pseudolites with 15 m transmitting antennas, and 1 m user antennas. A single fixed Gaussian hotspot has $\sigma_h = 6$ km, with two fixed convex obstacles outside its core. Table I lists the physical and service settings.

Scene coordinates use $\mathbf{q}_0 = (0, 0, -R)^{\mathsf{T}}$ and the global x, y tangent axes. The hotspot is $\mathbf{q}_h = \mathrm{Exp}_{\mathbf{q}_0}(E_0[3000 \;\; 1000]^{\mathsf{T}})$ in meters. Obstacle centers $\mathbf{s}_j$ use exponential coordinates at $\mathbf{q}_h$, with the first tangent axis given by the projected global $+x$ direction and the second oriented toward $+y$. Each obstacle is the exposed cap of a buried closed ball. For footprint geodesic radius a_j and height h_j, its three-dimensional parameters are

$$T_j = R + h_j, \qquad \ell_j = \frac{T_j^2 - R^2}{2[T_j - R\cos(a_j/R)]}, \qquad \mathbf{C}_j = \frac{\ell_j}{R}\mathbf{s}_j, \qquad r_j = T_j - \ell_j. \tag{21}$$

Rover placement excludes $d_g(\mathbf{p}_i, \mathbf{s}_j) \le a_j$.

For full-rank geometry, the utility is

$$f(D) = 0.20 + 0.8\frac{16}{16 + D^2}. \tag{22}$$

PSO uses 40 particles, inertia 0.7, $c_1 = c_2 = 1.5$, a coordinate velocity cap of 2000 m, a budget of 6000 objective evaluations, and a generation ceiling of 300.

The search grid contains 5376 nodes, with eight radial quadrature nodes per subinterval and 96 angular nodes. Doubling both resolutions produces the 21504-node reporting grid; a second doubling produces the 86016-node refinement grid. Each grid retains surface area weights and Gaussian normalization. Final configurations pass refinement when $|H_{86016} - H_{21504}| \le \max(0.002, 0.01|H_{86016}|)$. All twenty passed, with a maximum absolute difference of 5.78×10^{-4}. Objective histories and final statistics use the reporting grid.

TABLE I
Static Simulation Parameters

Parameter	Value
Lunar radius	1737.4 km
Cap geodesic radius	50 km
Number of rovers	10
Transmitter / user height	15 m / 1 m
Hotspot / demand	One; $\sigma_h = 6$ km
Artificial obstacles	Two convex caps
Minimum separation	10 m
Low service levels	0.02, 0.08, 0.14, 0.20
Full-rank map	Rational ($D_0 = 4$)
Independent random trials	20

Obstacle	Center coordinates (km)	a_j (km)	h_j (m)
East	$(8.5, 0)$	1.5	120
Southwest	$(-10.5/\sqrt{2}, -10.5/\sqrt{2})$	1.2	100

Fig. 2 shows representative initial and optimized configurations and the final service field over the entire cap and hotspot region.

The optimized rovers concentrate around the hotspot while satisfying obstacle and separation constraints. The resulting service field shows high utility across much of the high-demand region.

B. Independent Random Trials and Statistical Evaluation

Twenty independent seeds generate feasible initial swarms over the cap and determine the stochastic PSO coefficients for each trial. The scene, hotspot, service mapping, constraints, quadrature settings, and PSO parameters are held fixed, so variation across trials reflects initialization and stochastic search.

For each trial, the best stored configurations are evaluated on the common reporting grid at recorded checkpoints. Histories use cumulative objective evaluations as the horizontal axis and retain each recorded value until the next checkpoint, without smoothing. Fig. 3 shows the mean objective and minimum-to-maximum range across the twenty trials. Reported histories can be nonmonotone because the reporting and search grids differ.

The mean objective rises rapidly before approaching a plateau. The narrower final minimum-to-maximum band indicates more concentrated terminal values across the twenty trials under the fixed search budget.

Table II reports the final objective and search runtime for the twenty complete trials. Standard deviations use denominator $20 - 1$. Search runtime was measured in MATLAB R2025b Update 2 and excludes reporting-grid evaluations, saving, and plotting.

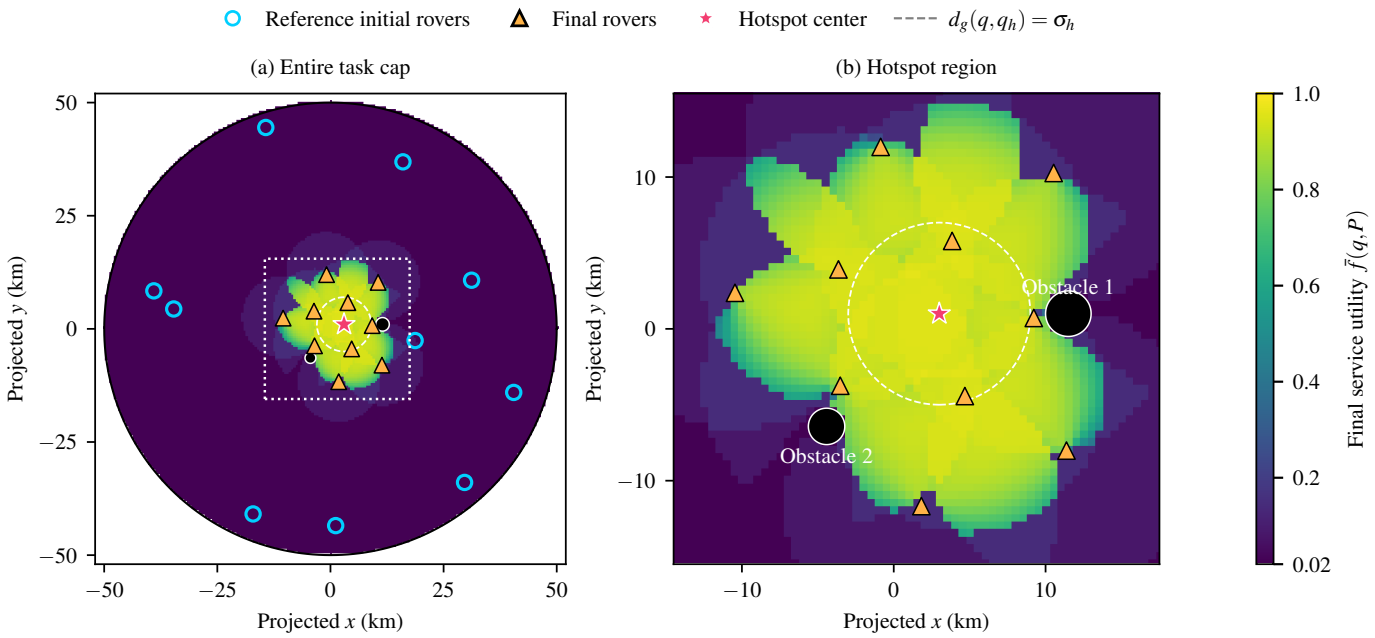

Fig. 2. Representative initial and optimized rover configurations and the final GDOP-based service field: (a) entire task cap and (b) hotspot region. The reference initial configuration is one initial swarm member, distinct from the initial swarm best used in Fig. 3.

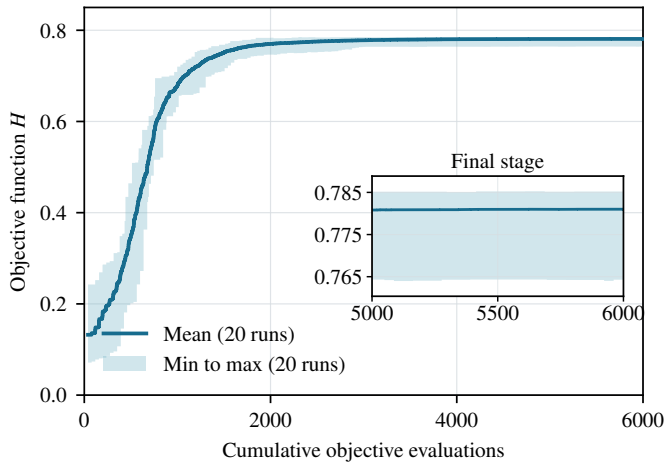

Fig. 3. Statistical evolution of the spherical objective over twenty independent PSO trials.

TABLE II
STATISTICAL RESULTS OVER TWENTY INDEPENDENT TRIALS

Quantity	Mean	Std.	Min	Max
Final objective H	0.780976	0.005668	0.764288	0.785200
Search runtime (s)	24.72	1.13	21.94	26.73

V. CONCLUSION

This paper combines hard visibility and clock-bias-aware, surface-constrained GDOP in a demand-weighted coverage model for lunar pseudolite deployment. Derivative-free PSO searches feasible static configurations. Twenty independent trials with 6000 objective evaluations each yielded a mean final objective of 0.780976 and a sample standard deviation of 0.005668. Future work will address online reconfiguration under failures and shifting demand.

REFERENCES

[1] NASA, *LunaNet Interoperability Specification*, ver. 5, Jan. 2025. [Online]. Available: https://www.nasa.gov/directorates/somd/space-communications-navigation-program/lunanet-interoperability-specification/

[2] European Space Agency, "ESA launches Moonlight to establish lunar communications and navigation infrastructure," Oct. 15, 2024. [Online]. Available: https://www.esa.int/Newsroom/Press_Releases/ESA_launches_Moonlight_to_establish_lunar_communications_and_navigation_infrastructure

[3] F. Pereira, P. M. Reed, and D. Selva, "Multi-objective design of a lunar GNSS," *NAVIGATION*, vol. 69, no. 1, 2022, Art. no. navi.504, doi: 10.33012/navi.504.

[4] W. W. Jun, K.-M. Cheung, E. G. Lightsey, and C. Lee, "A minimal architecture for real-time lunar surface positioning using joint Doppler and ranging," *IEEE Trans. Aerosp. Electron. Syst.*, vol. 58, no. 2, pp. 1367–1376, Apr. 2022, doi: 10.1109/TAES.2021.3122876.

[5] B. T. Wallace *et al.*, "A lunar surface pseudolite architecture for regional communication and radionavigation," *IEEE Trans. Aerosp. Electron. Syst.*, vol. 61, no. 3, pp. 5611–5634, Jun. 2025, doi: 10.1109/TAES.2024.3520536.

[6] C. Toldbo, A. Kiss, N. Törjék, C. A. T. Vázquez, D. Bényei, and M. Therkelsen, "Deployment method and optimal placement of surface beacon navigation system for co-located lunar landings," *Acta Astronaut.*, vol. 193, pp. 432–443, 2022, doi: 10.1016/j.actaastro.2022.01.003.

[7] W. Tang, J. Chen, C. Yu, J. Ding, and R. Wang, "A new ground-based pseudolite system deployment algorithm based on MOPSO," *Sensors*, vol. 21, no. 16, 2021, Art. no. 5364, doi: 10.3390/s21165364.

[8] J. Cortés, S. Martínez, T. Karatas, and F. Bullo, "Coverage control for mobile sensing networks," *IEEE Trans. Robot. Autom.*, vol. 20, no. 2, pp. 243–255, Apr. 2004, doi: 10.1109/TRA.2004.824698.

[9] S. Martínez and F. Bullo, "Optimal sensor placement and motion coordination for target tracking," *Automatica*, vol. 42, no. 4, pp. 661–668, Apr. 2006, doi: 10.1016/j.automatica.2005.12.018.

[10] L. Zhang, Z. Zhang, R. Siegwart, and J. J. Chung, "Distributed PDOP coverage control: Providing large-scale positioning service using a multi-robot system," *IEEE Robot. Autom. Lett.*, vol. 6, no. 2, pp. 2217–2224, Apr. 2021, doi: 10.1109/LRA.2021.3059625.

[11] S. Bhattacharya, R. Ghrist, and V. Kumar, "Multi-robot coverage and exploration on Riemannian manifolds with boundaries," *Int. J. Robot. Res.*, vol. 33, no. 1, pp. 113–137, Jan. 2014, doi: 10.1177/0278364913507324.

[12] H.-T. Zhang, J. Zou, and X. Liu, "Cooperative optimal surface coverage control of multi-agent systems in non-convex surface environments," *Automatica*, vol. 185, 2026, Art. no. 112808, doi: 10.1016/j.automatica.2025.112808.

[13] M. P. do Carmo, *Riemannian Geometry*. Boston, MA, USA: Birkhäuser, 1992.

[14] J. Kennedy and R. Eberhart, "Particle swarm optimization," in *Proc. IEEE Int. Conf. Neural Networks*, vol. 4, 1995, pp. 1942–1948, doi: 10.1109/ICNN.1995.488968.

[15] Y. Shi and R. Eberhart, "A modified particle swarm optimizer," in *Proc. IEEE Int. Conf. Evol. Comput.*, 1998, pp. 69–73, doi: 10.1109/ICEC.1998.699146.